coatings

MDPI

Communication

Preparation and Characterization of Pulse Electrodeposited Ni/W-SiC Nanocomposite Coating on Mild Steel Substrate

Zhaoge Zhu [1,*], Longqing Zou [1], Huaxing Li [1] and Hongbin Zhang [2]

[1] College of Mechanical Science and Engineering, Northeast Petroleum University, Daqing 163318, China
[2] School of Mechatronics Engineering, Qiqihar University, Qiqihar 161006, China
* Correspondence: zhaogezhu104@npu.edu.cn

Abstract: In order to improve the performances of metal containers, furnace bodies and agricultural tools manufactured by mild steels, Ni/W-SiC nanocomposites are prefabricated on mild steel substrate by the pulse electrodeposition (PED) method. The morphology, texture, microstructure, microhardness, and wear performances of Ni/W-SiC nanocomposites are examined by scanning electron microscopy (SEM), atomic force microscopy (AFM), X-ray diffraction (XRD), dispersive X-ray spectroscopy (EDX), hardness tester, and friction wear testing. The results indicate that the SiC size in nanocomposites is ~32.4 nm when its concentration in electrolytes is 7 g/L. The S1 and S4 nanocomposites' microstructures (the S1 composite was prefabricated at 4 g/L, and the S4 composite was deposited at 13 g/L) reveal many large cauliflower-shaped grains. However, the S2 nanocomposite (the S2 composite was obtained at 7 g/L) demonstrates the homogeneous, finest and smoothest surface morphology. The diffraction angles of S1 nanocomposite are 41.2°, 51.7°, and 71.2° depicting the sharpest diffraction peaks, corresponding to the (1 1 1), (2 0 0), and (2 2 0) crystal planes of Ni-W grains, respectively. Moreover, the S2 nanocomposite exhibits the lowest wear depth and width of 34.2 μm and 5.5 mm, respectively. Some shallow and fine scratches on the as-described nanocomposites' surface indicate its excellent tribological performance. However, the S4 nanocomposite exhibits a wear depth of 86.3 μm and a width of 11.9 mm.

Keywords: characterization; Ni/W-SiC nanocomposite; X-ray diffraction; wear performance; pulse electrodeposition

check for updates

Citation: Zhu, Z.; Zou, L.; Li, H.; Zhang, H. Preparation and Characterization of Pulse Electrodeposited Ni/W-SiC Nanocomposite Coating on Mild Steel Substrate. *Coatings* **2023**, *13*, 484. https://doi.org/10.3390/coatings13030484

Academic Editor: Eva Pellicer

Received: 27 January 2023
Revised: 10 February 2023
Accepted: 13 February 2023
Published: 21 February 2023

Copyright: © 2023 by the authors. Licensee MDPI, Basel, Switzerland. This article is an open access article distributed under the terms and conditions of the Creative Commons Attribution (CC BY) license (https://creativecommons.org/licenses/by/4.0/).

1. Introduction

Recently, Ni-W composites have gained notable attention for improving surface performances of machine parts, industrial pumps, oil rods, and metal vanes due to their excellent anti-corrosion and wear capabilities [1–3]. The wear and corrosion resistances are greatly enhanced when the Ni-W composites are coated on the metal parts. Many methods are designed to deposit Ni-W nanocomposites, including electrodeposition, jet electrodeposition, and chemical deposition [4,5]. Generally, electrodeposition is the most commonly used method to prefabricate Ni-W nanocomposites due to its simple operation, low cost, and high deposition rate. The pulse electrodeposition (PED) method is one of electrodeposition technique, and the advantages can be listed as follows: (1) the plating rate and coating surface area are large; (2) the current is frequently connected and disconnected, and the coating grains grow intermittently; (3) the current efficiency is high, and the preparation cost is low. The preparation of Ni/W-based nanocomposites via PED has recently attracted wide attention. For example, Popczyk et al. [6] successfully prepared Zn/Ni-P-W composites using the PED method and discussed the effect of W content on the microhardness of composites. Li et al. [7] prepared Ni/W-SiC nanocomposites on mild steel substrates. They found that the incorporation of SiC nanoparticles could alter the composition of Ni-W composites. Krasikov et al. [8] studied the microstructure and performance of Ni-40%W deposited by the PED technique. Similarly, Xia et al. [9] examined the current density effect

on the microstructure and wear performance, indicating that the structure and composition of Ni-TiN nanocomposites were determined by the current density.

It is generally known that SiC particles exhibit high strength, outstanding stability, and excellent properties [10–13]. Therefore, these particles were embedded into Ni/W-based nanocomposites to improve the capability of the nanocomposites. Several reports have appeared on Ni/W-based nanocomposites; however, only a few reports have analyzed the effect of SiC content on the surface and cross-section structures, microhardness, and wear properties of Ni/W-SiC nanocomposites. Therefore, the preparation and characterization of pulse-electrodeposited Ni/W-SiC nanocomposites should be discussed in detail. This study focuses on depositing Ni/W-SiC nanocomposites on mild steel substrates via the PED and examines their surface and cross-section structures, microhardness, and wear properties. A new idea is proposed to protect mild steel by extending the service life of machine parts, industrial pumps, oil rods, and metal vanes. Hence, Ni/W-SiC nanocomposites are manufactured on a mild steel surface using the PED method. In addition, the influence of the SiC content on the surface and cross-section structures, phase structure, microhardness, and wear performances of Ni/W-SiC nanocomposites is surveyed by various analytical techniques and friction wear testing.

2. Experiment and Characterization

Before the PED experiment, a mild steel substrate was utilized as a cathode (50 × 30 × 5 mm^3), and a 99.998% pure nickel plate acted as the anode (100 × 60 × 10 mm^3). Generally, the mild steels were applied to fabricate metal containers, furnace bodies, and agricultural tools [14]. The nickel plate and mild steel were firstly polished with 200, 500, 800, 1000, and 2000-grit abrasive papers by hand. Then, they were burnished using a W960 type automatic polishing machine (Qingdao Polishing Machine Factory). The chemical composition of the mild steel was 98.47 wt.% Fe, 1.05 wt.% Mn, 0.22 wt.% Si, 0.17 wt.% Cr, 0.046 wt.% C, 0.013 wt.% P, and 0.031 wt.% Nb. Tables 1 and 2 display the composition of the bath solution and the plating parameters for Ni/W-SiC nanocomposites, respectively.

Table 1. Composition of the bath solution for depositing Ni/W-SiC nanocomposites.

Compositions	Parameters
$Na_2WO_4 \times 2H_2O$ (g/L)	30
$NiSO_4 \times 6H_2O$ (g/L)	58
$C_6H_8O_7 \times H_2O$ (g/L)	65
NH_3H_2O (mg/L)	70
SiC concentration (g/L)	4, 7, 10, 13
pH	4.5
Temperature (°C)	46

Table 2. Plating parameters used in the PED experiment.

Plating Parameters	Parameters
Peak current density (A/dm^2)	35
Duty cycle	25%
Frequency (Hz)	250
Average current density (A/dm^2)	6.2
Plating time (min)	40

Figure 1 indicates the surface morphology purchased from Shanghai Kedi Nano Technology Co., Ltd., Shanghai, China. The grain distribution of SiC nanoparticles is presented in the top right corner of Figure 1. It is clearly that SiC nanoparticles have regular and granular black particles with a mean size of ~32.4 nm. A DEM-100A plating power supply (Shenzhen Keda Technology Co., Ltd., Shenzhen, China) was applied to deposit the Ni/W-SiC nanocomposites in the PED process. A DX-500 ultrasonic cleaner (Beijing

Daixia Technology Co., Ltd., Beijing, China) was utilized to agitate the plating solution at an ultrasonic power of 200 W for 20 min. After the test, Ni/W-SiC nanocomposites were washed with alcohol, acetone, and distilled water. The composites were prefabricated at SiC additions of 4, 7, 10, and 13 g/L in the electroplate liquid and were noted as S1, S2, S3, and S4 nanocomposites, respectively.

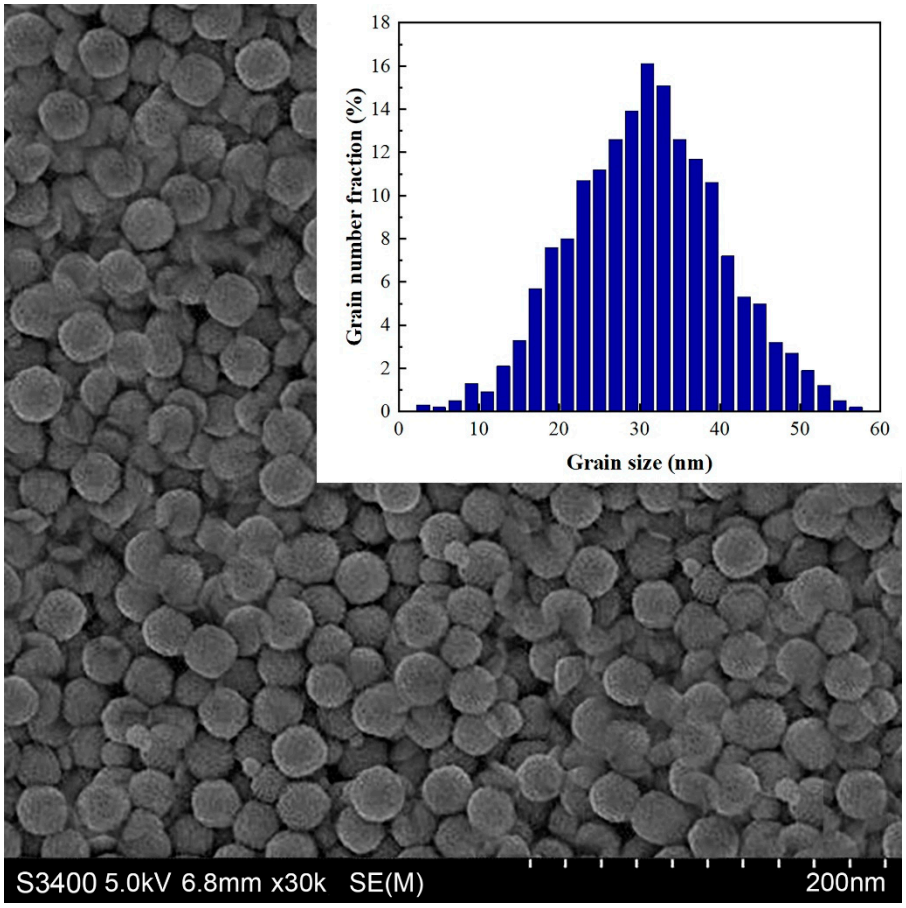


Figure 1. SEM image of SiC nanoparticles.

The surface and cross-section microstructures, phase structure, and surface roughness of the Ni/W-SiC nanocomposites were detected by using S3400 type SEM (Hitachi High-Tech. Co., Ltd., Tokyo, Japan), XRD-7000 type XRD (Shimadzu Co., Ltd., Kyoto, Japan), INCA EDX (Oxford Co., Ltd., Oxford, UK), and EPMA-8050 type AFM (Shimadzu Co., Ltd.). In the SEM test, the acceleration voltage was 20 kV, the magnification was 15–200,000, and the resolution ratio was 6 nm. The Ni/W-SiC nanocomposite samples were cut by a DK7740E wire cutting machine (Taizhou Jinggong High-Tech. Co., Ltd., Taizhou, China), and then the cross-section images of the samples could be observed. In the AFM experiment, the scanning pattern was tapping mode, the probe was silicon nitride, and the lateral resolution was 0.2 nm. In the XRD measurement, a Cu target was utilized with a tube voltage of 30 kV, and the scanning step was 0.01°. The X-ray wavelength was 0.15406 nm, and the diffraction angle was set at 20°~90°. The Ni/W grain diameter (D) was estimated using the Equation (1) as follows:

$$D = 0.89\lambda/(\beta\cos\theta) \quad (1)$$

where λ is the X-ray wavelength; β represents the full width at half maximum of diffraction peaks; and θ shows the Bragg angle.

The MH-650 hardness tester (Shandong Celiang Technology Co., Ltd., Linyi, China) was utilized to estimate the microhardness of Ni/W-SiC nanocomposites. Six positions were randomly determined on the nanocomposites' surface to examine the microhardness. The applied force was 1 N for 15 s of applied time. The wear performance of Ni/W-SiC nanocomposites was examined by using a GPX-3A type wear tester (Shandong Jingcheng Technology Co., Ltd., Shandong, China) using the following parameters: friction moment: ±0.002 N·m, spindle speed error: ±2 rpm. A carbide steel ball acted as the friction pair with a surface hardness of 62 HRC, and the applied load was 3 N. The wear rate and wear time were 0.15 m/s and 60 min, respectively. After the wear test, the worn structures of nanocomposites were observed by SEM. A BS220 electronic balance (Germany Sartorius Co., Ltd., Goettingen, Germany, accuracy: 0.1 mg) was utilized to test the loss mass of the nanocomposites.

3. Results and Discussion

3.1. Surface Morphology Observation

Figure 2a–h demonstrate the cross-section structures and SiC contents in S1, S2, S3, and S4 nanocomposites, respectively. The Ni/W-SiC nanocomposites prepared using PED are tightly bonded to the substrate's surface, with no obvious grooves, cracks, or other defects at the interface. The thicknesses of S1, S2, S3, and S4 nanocomposites are 43.1 µm, 47.7 µm, 47.1 µm, and 45.3 µm, respectively. The more uniform and dense microstructure of the cross-section of S2 nanocomposite illustrates that PED could successfully prepare smooth composites under the optimal SiC content (7 g/L) in the plating solution.

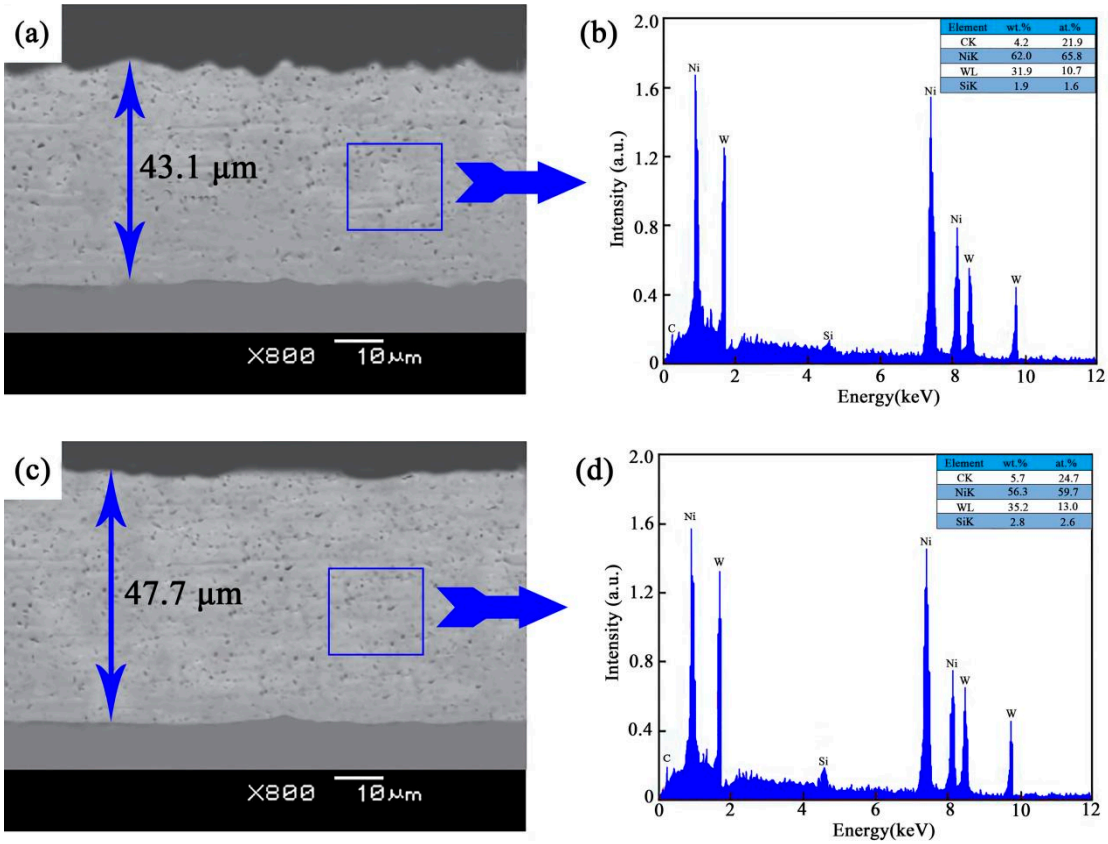


Figure 2. *Cont.*

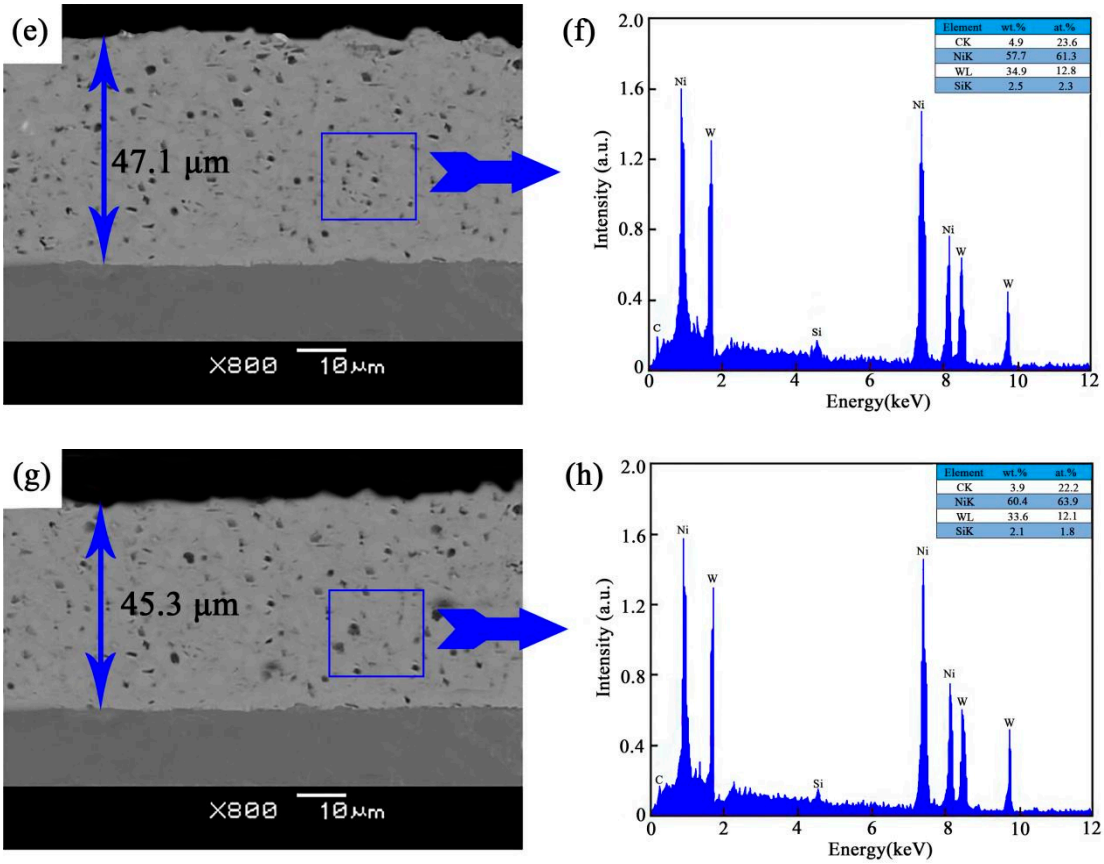


Figure 2. Cross-section SEM images of Ni/W-SiC nanocomposites: (**a**) S1, (**c**) S2, (**e**) S3, and (**g**) S4 nanocomposites, and SiC contents in Ni/W-SiC nanocomposites: (**b**) S1, (**d**) S2, (**f**) S3, and (**h**) S4 nanocomposites.

Si contents in S1, S3, and S4 nanocomposites are 1.9 wt.%, 2.5 wt.%, and 2.1 wt.%, respectively. The C contents in S1, S3, and S4 nanocomposites are 4.2 wt.%, 4.9 wt.%, and 3.9 wt.%, respectively. However, S2 has the maximum Si and C concentration (2.8 wt.% and 5.7 wt.%), indicating that a proper SiC concentration contributes to the SiC deposition in the Ni/W-SiC composite. These conclusions indicate that many SiC nanoparticles are successfully embedded in Ni/W-SiC nanocomposites.

Figure 3 reveals the effect of the SiC content in the electroplate liquid on the surface morphology of Ni/W-SiC nanocomposites. Numerous irregular clusters appeared on the surfaces of S1 and S4 composites; however, the S3 nanocomposite has a smoother and finer microstructure among the three composites. In addition, the S2 nanocomposite appears to possess the smoothest and most homogeneous surface morphology among all four composites (see Figure 3b). These results are explained by the fact that a suitable SiC concentration (7 g/L) in the electroplate liquid promotes the dispersion of SiC nanoparticles and increases the co-deposition rate of Ni ions, W ions, and SiC nanoparticles. Furthermore, the SiC nanoparticles in the S2 nanocomposite hinder the growth of Ni grains, bringing about a smooth surface morphology [14].

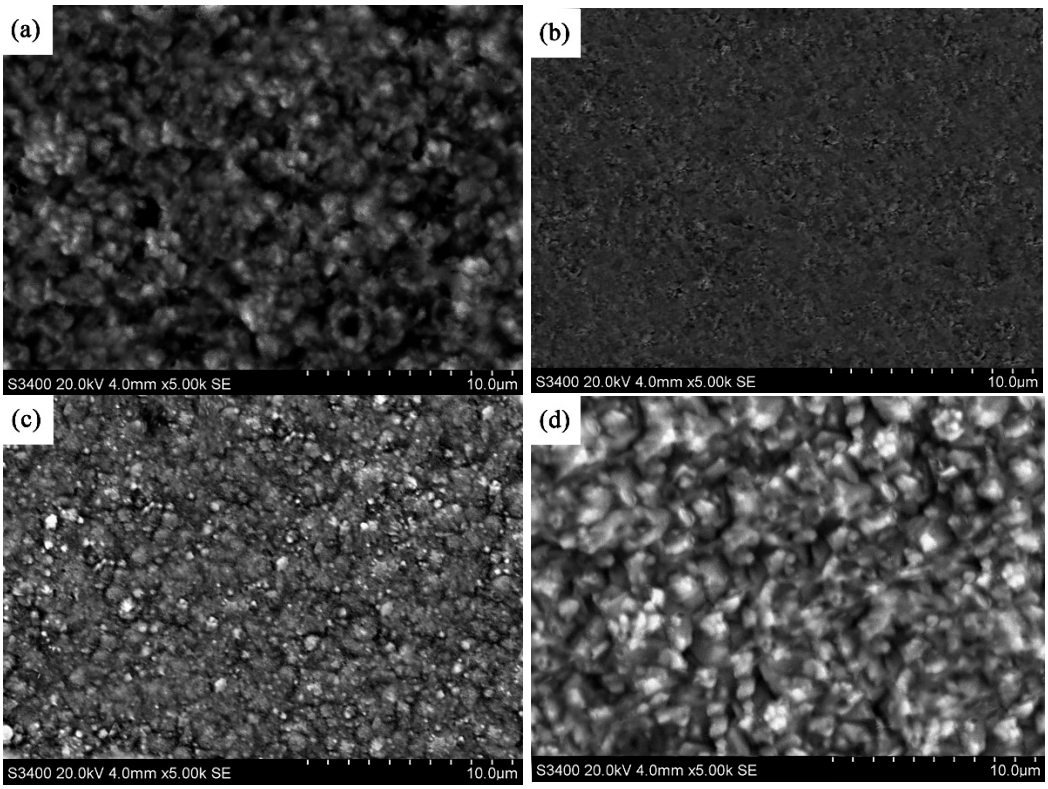


Figure 3. Effect of the SiC content in the electroplate liquid on the surface morphology of Ni/W-SiC nanocomposites: (**a**) 4 g/L, (**b**) 7 g/L, (**c**) 10 g/L, and (**d**) 13 g/L.

3.2. AFM Survey

Figure 4 presents the AFM images of S2 and S4 nanocomposites obtained by using PED technique. The S2 nanocomposite possesses an even surface, and the depths of protrusion heights and depression are 78.5 nm and 109.7 nm, respectively (see Figure 4b). However, the microstructures of the S4 nanocomposite are rough and irregular, and the depths of protrusion heights and depression are 119.3 nm and 188.9 nm, respectively (Figure 4d), testifying to the smooth and even Ni/W-SiC nanocomposite deposited at an SiC concentration of 7 g/L. The results are similar to the phenomena described by Cai et al. [15].

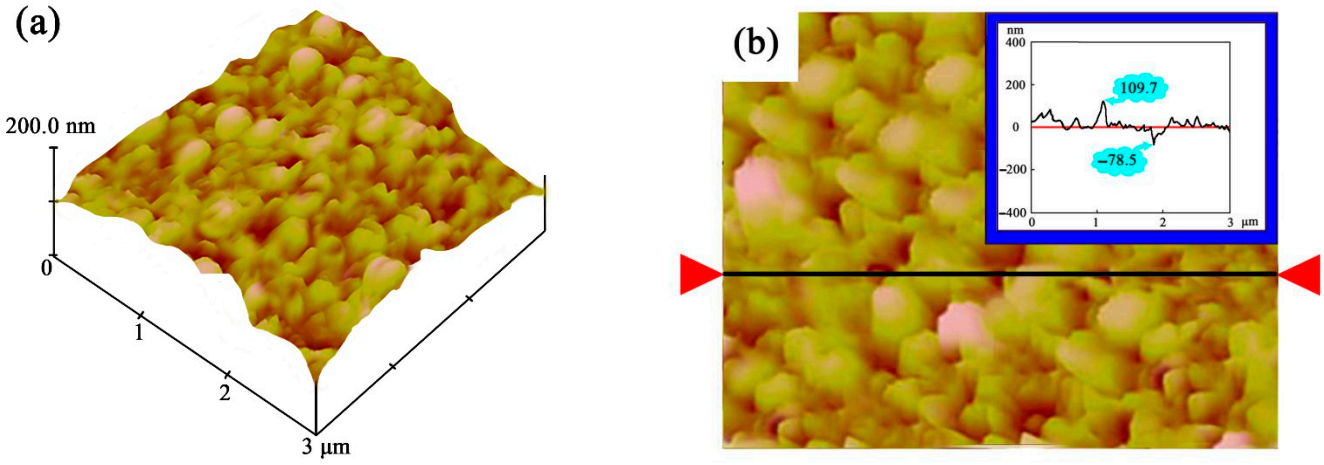


Figure 4. *Cont.*

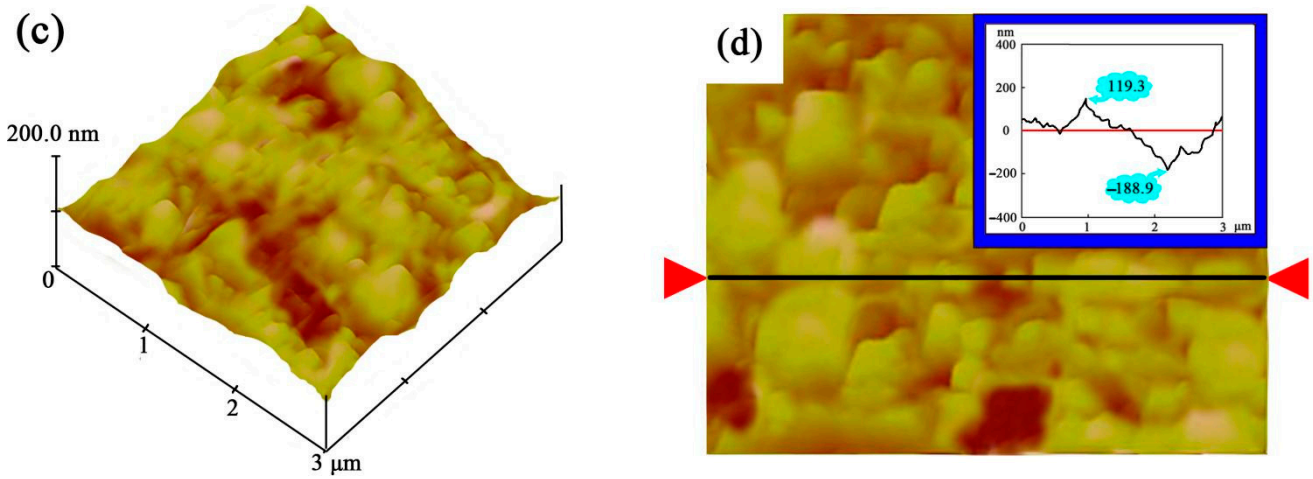


Figure 4. AFM pictures of three dimensional morphologies: (**a**) S2 and (**c**) S4 nanocomposites; AFM pictures of two dimensional morphologies: (**b**) S2 and (**d**) S4 nanocomposites.

3.3. XRD Measurement

The effect of SiC content in the electrolyte on XRD spectrograms of Ni/W-SiC nanocomposites is exhibited in Figure 5. In the S1 nanocomposite, the diffraction angles of Ni-W grains are 41.2°, 51.7°, and 71.2° with the sharpest diffraction peaks among four nanocomposites, corresponding to (1 1 1), (2 0 0), and (2 2 0) planes, respectively. When the SiC content rises from 4 g/L to 7 g/L, the diffraction peaks' width of Ni-W grains in the S1 nanocomposite is wider than in the S2 nanocomposite. With a further increase in SiC content, the diffraction peaks become sharper than those of the S2 nanocomposite, illustrating that when the SiC content in the electrolyte increases from 7 g/L to 10 g/L, this leads to the decrease in peak diffraction of Ni-W grains. In contrast, the Ni-W contents in the S4 nanocomposite increase evidently with the SiC content increasing from 7 to 13 g/L, and the corresponding Ni-W peak intensity increases (see Figure 5d). Moreover, three low-intensity diffraction peaks (diffraction angles: 37.2°, 42.6°, and 62.3°) are detected in the nanocomposites mentioned above in the XRD curves, testifying that the SiC particles successfully embed in Ni/W-SiC composites, as reported by Wang et al. [16].

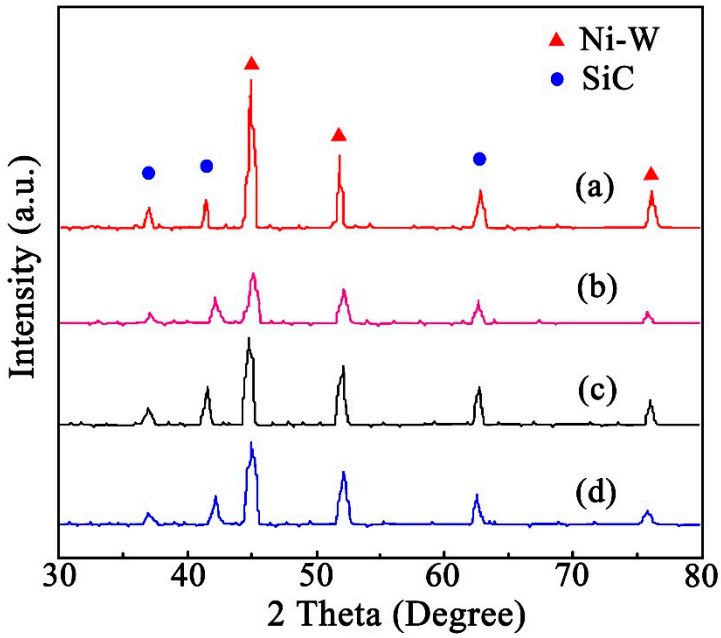


Figure 5. XRD spectrograms of (**a**) S1, (**b**) S2, (**c**) S3, and (**d**) S4 nanocomposites.

From Equation (1) and Figure 5, the average grain sizes of the Ni/W-SiC nanocomposites are calculated, as shown in Table 3. The average Ni-W sizes of the S2 and S4 nanocomposites are about 84.3 nm and 147.6 nm, respectively. These results show that when the SiC content in the bath solution is optimum (7 g/L), more nucleation points are available for Ni-W grains, beneficial to the prefabrication of fine and even Ni/W-SiC nanocomposites [17]. When the SiC content in the solution is lower, only a few SiC nanoparticles are embedded into Ni/W-SiC composites, and the number of Ni-W grains is few, bringing about the presence of larger Ni-W grains in Ni/W-SiC composites. Moreover, when the SiC content in the solution is higher (13 g/L), numerous SiC nanoparticles agglomerate, reducing the nucleation points of Ni-W grains, resulting in larger Ni-W grain sizes in Ni/W-SiC composites.

Table 3. Average Ni-W sizes of Ni/W-SiC nanocomposites.

Composite Type	Mean Ni/W Grain Size (nm)
S1	135.8
S2	84.3
S3	111.4
S4	147.6

3.4. Microhardness Analysis

Figure 6 displays the microhardnesses of four Ni/W-SiC nanocomposites deposited at SiC concentrations of 4 g/L, 7 g/L, 10 g/L, and 13 g/L. The SiC content in the bath solution affects the microhardness of composites [18]. The average microhardness value of the S2 nanocomposite is ~905.3 HV. Under optimal SiC concentration, SiC nanoparticles are uniformly embedded in the Ni/W-SiC composites, enhancing the Ni-W grains' fine crystal reinforcement [19]. These results indicate that the microhardness of the S2 nanocomposite is significantly increased, attributed to the high microhardness of SiC nanoparticles (~21 GPa) [20]. In contrast, the average hardness values of the S1 and S4 nanocomposites are only ~745.6 and ~771.8 HV, respectively. This phenomenon is because the SiC contents of 4 g/L and 13 g/L in the solution could not extensively refine the Ni-W grains; thus, the microhardness value of the Ni/W-SiC nanocomposites decreased. These results are consistent with the research reported by Liu et al. [21].

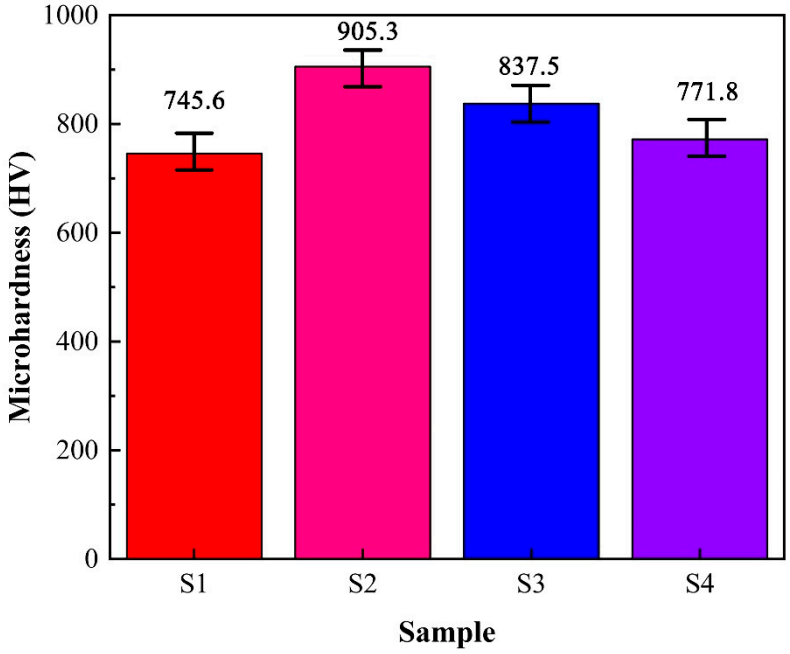


Figure 6. Microhardnesses of Ni/W-SiC nanocomposites.

3.5. Friction Performance Test

Figure 7 presents the wear curves of the obtained S1, S2, and S4 nanocomposites at room temperature. Among the as-prepared nanocomposites, the S1 exhibits the deepest wear depth of 109.8 μm and the largest wear width of 10.8 mm. However, the S2 exhibits the lowest wear depth and width of 34.2 μm and 5.5 mm, and those of the S4 nanocomposite are 86.3 μm and 11.9 mm, respectively. Some wide and deep grooves are found on the surface of the S1 nanocomposite, illustrating that this nanocomposite indicates the worst friction performance. In contrast, some grooves and accumulations are observed on the wear surface of the S4 composite. However, only a few narrow and shallow scratches are discovered on the S2 surface, certifying that this nanocomposite has outstanding wear-resisting properties. The degree of wear is usually inversely proportional to its microhardness [22]. In this study, the hardness of the S2 nanocomposite is the highest, proving its prominent friction resistance. These results are consistent with that discussed by Bratu et al. [23].

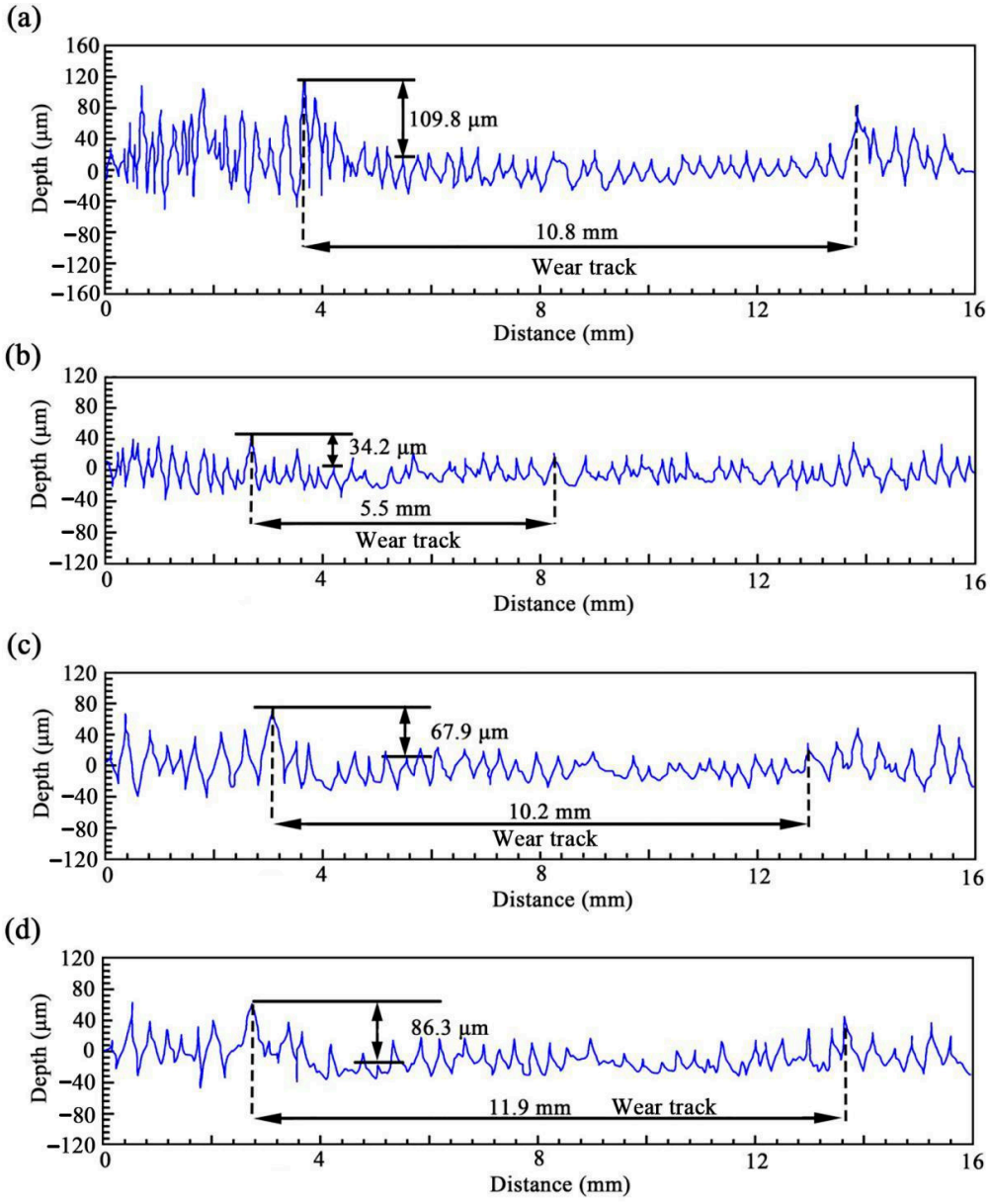


Figure 7. Wear curves of (**a**) S1, (**b**) S2, (**c**) S3, and (**d**) S4 nanocomposites.

4. Conclusions

1. The S1 and S4 nanocomposites' microstructures reveal many large cauliflower-shaped grains. The S2 nanocomposite demonstrates the most homogeneous, finest, and smoothest surface morphology. The smooth surface structure of the S2 nanocomposite has depths of depression, and protrusion heights are 78.5 nm and 109.7 nm, respectively.
2. The diffraction angles of the S1 nanocomposite are 41.2°, 51.7°, and 71.2° depicting the sharpest diffraction peaks, corresponding to the (1 1 1), (2 0 0), and (2 2 0) crystal planes of Ni-W grains, respectively. In addition, the average hardness of the S2 nanocomposite is ~905.3 HV.
3. The S2 nanocomposite exhibits the lowest wear depth and width of 34.2 μm and 5.5 mm, respectively. Some wide and deep grooves are observed on the surface of the S1 nanocomposite, indicating that this nanocomposite exhibits the worst friction performance.

Author Contributions: Methodology, Z.Z. and H.L.; validation, L.Z. and H.Z.; formal analysis, Z.Z.; investigation, L.Z.; writing—original draft preparation, Z.Z.; writing—review and editing, L.Z. All authors have read and agreed to the published version of the manuscript.

Funding: The research is supported by the National Natural Science Foundation of China (Granted no. 51974089) and the Key Project of the "Ten Four Five" Plan of Education Science in Heilongjiang Province (Granted no. GJB1421101).

Institutional Review Board Statement: Not applicable.

Informed Consent Statement: Not applicable.

Data Availability Statement: Not applicable.

Conflicts of Interest: The authors declare no conflict of interest.

References

1. Dilek, S.; Algül, H.; Akyol, A.; Alp, A.; Akbulut, H.; Uysal, M. Pulse electro co-deposition of submicron-sized TiC reinforced Ni–W coatings: Tribological and corrosion properties. *J. Asian Ceram. Soc.* **2021**, *9*, 673–685. [CrossRef]
2. Li, H.; He, Y.; Luo, P.; Xue, S.; Li, Z.; Cheng, X.; Zhong, J.; Yan, L.; Fan, Y. Synthesis of ZrB2 strengthened Ni W composite coating and study of its mechanical characters and anti-corrosion performance. *Surf. Coat. Technol.* **2022**, *441*, 128553. [CrossRef]
3. Zhang, C.; Zhang, B.; Xie, L. Improving mechanical properties of Ni-W based nanocrystalline films by multilayered architecture. *Surf. Coat. Technol.* **2020**, *402*, 126341. [CrossRef]
4. Xu, J.; Li, Z.; Zhu, W.; Liu, Z.; Liu, W. The comparative study of thermal fatigue behavior of laser deep penetration spot cladding coating and brush plating Ni–W–Co coating. *Appl. Surf. Sci.* **2006**, *253*, 2618–2624. [CrossRef]
5. Li, C.; Xia, F.; Ma, C.; Li, Q. Research on the corrosion behavior of Ni-SiC nanocoating prepared using a jet electrodeposition technique. *J. Mater. Eng. Perform.* **2021**, *5*, 1–9. [CrossRef]
6. Popczyk, M.; Niedbaa, J. Characterization of corrosion resistance of Zn-Ni-W and Zn-Ni-P-W heat-treated coatings. *Inżynieria Powierzchni* **2021**, *25*, 13–17. [CrossRef]
7. Li, B.; Zhang, W.; Zhang, W.; Huan, Y. Preparation of Ni-W/SiC nanocomposite coatings by electrochemical deposition. *J. Alloys Compd.* **2017**, *702*, 38–50. [CrossRef]
8. Krasikov, A.V.; Bykova, A.D.; Merkulova, M.V.; Markov, M.A. Electrochemical deposition of nanocrystalline Ni–W coatings from citrate electrolytes. *Vopr. Mater.* **2020**, *1*, 111–117. [CrossRef]
9. Xia, F.; Li, C.; Ma, C.; Li, Q.; Xing, H. Effect of pulse current density on microstructure and wear property of Ni-TiN nanocoatings deposited via pulse electrodeposition. *Appl. Surf. Sci.* **2021**, *538*, 148139. [CrossRef]
10. Wasekar, N.; Latha, S.M.; Ramakrishna, M.; Rao, D.; Sundararajan, G. Pulsed electrodeposition and mechanical properties of Ni-W/SiC nano-composite coatings. *Mater. Des.* **2016**, *112*, 140–150. [CrossRef]
11. NWasekar, P.; Bathini, L.; Ramakrishna, L.; Rao, D.S.; Padmanabham, G. Pulsed electrodeposition, mechanical properties and wear mechanism in Ni-W/SiC nanocomposite coatings used for automotive applications. *Appl. Surf. Sci.* **2020**, *527*, 146896. [CrossRef]
12. Lin, C.; Chen, K.; He, J. The cavitation erosion behavior of electroless Ni-P-SiC composite coating. *Wear* **2006**, *261*, 1390–1396. [CrossRef]

13. Zhang, Z.; Xian, J.; Wu, H.; Jin, M.; Shen, Z. Influence of particle concentration on the elemental penetration region and properties of Ni-P-SiC composite coatings prepared through sandblasting and scanning electrodeposition on 45 steel surfaces. *Coatings* **2021**, *11*, 1237. [CrossRef]
14. Sfaira, M.; Srhiri, A.; Keddam, M.; Takenouti, H. Corrosion of a mild steel in agricultural irrigation waters in relation to partially blocked surface. *Electrochim. Acta* **1999**, *44*, 4395–4402. [CrossRef]
15. Cai, C.; Yin, J.; Zhang, Z.; Yang, J. The electrodeposition of nanostructured Ni-TiN composite films. *Mater. Sci. Forum* **2009**, *620–622*, 727–730. [CrossRef]
16. Wang, P.; Cheng, Y.; Zhang, Z. A study on the electrocodeposition processes and properties of Ni-SiC nanocomposite coatings. *J. Coat. Technol. Res.* **2011**, *8*, 409–417. [CrossRef]
17. Xia, F.; Li, Q.; Ma, C.; Liu, W.; Ma, Z. Preparation and wear properties of Ni/TiN-SiC nanocoatings obtained by pulse current electrodeposition. *Ceram. Int.* **2020**, *46*, 7961–7969. [CrossRef]
18. Sun, C.; Liu, X.; Zhou, C.; Wang, C.; Cao, H. Preparation and wear properties of magnetic assisted pulse electrodeposited Ni-SiC nanocoatings. *Ceram. Int.* **2019**, *45*, 1348–1355. [CrossRef]
19. Zhang, H.; Xia, F.; Wang, J.; Xu, F. Influence of duty cycle and pulse frequency on structures and performances of electrodeposited Ni-W/TiN nanocomposites on oil-gas X52 steels. *Coatings* **2021**, *11*, 1182. [CrossRef]
20. Yang, X.; Zhang, M.; Huang, Y.; Hu, X.; Pan, Y.; Cheng, S.; Mu, D.; Ding, Y. Preparation and friction and wear resistance of SiC/Ni nano-composite coatings. *Mater. Mech. Eng.* **2014**, *38*, 53–57. [CrossRef]
21. Liu, W.; Jiang, K.; Li, Q.; Ma, C.; Xia, F. Jet pulse electrodeposited Ni-SiC thin coatings by using experimental system designed for potential industrial application. *Int. J. Electrochem. Sci.* **2021**, *16*, 21044. [CrossRef]
22. Lattanzi, L.; Etienne, A.; Li, Z.; Chandrashekar, G.; Gonapati, S.; Awe, S.; Jarfors, A. The effect of Ni and Zr additions on hardness, elastic modulus and wear performance of Al-SiCp composite. *Tribol. Int.* **2022**, *169*, 107478. [CrossRef]
23. Bratu, F.; Benea, L.; Celis, J. Tribocorrosion behaviour of Ni-SiC composite coatings under lubricated conditions. *Surf. Coat. Technol.* **2007**, *201*, 6940–6946. [CrossRef]

Disclaimer/Publisher's Note: The statements, opinions and data contained in all publications are solely those of the individual author(s) and contributor(s) and not of MDPI and/or the editor(s). MDPI and/or the editor(s) disclaim responsibility for any injury to people or property resulting from any ideas, methods, instructions or products referred to in the content.